Effect of Prompt Particle Events on OLCI Ocean Color Imagery in the South Atlantic Anomaly: Detection and Removal

Juan I. Gossn

IEEE Proof

***Abstract*— It has been found that cosmic rays and massive charged particles trapped in the magnetosphere or arriving from the sun might produce spike noise over the dark offset signal coming from charge-coupled devices (CCDs) on optic sensors such as Ocean and Land Color Instrument (Sentinel-3/OLCI) and Medium Resolution Imaging Spectrometer (Envisat/MERIS). These phenomena are called prompt particle events (PPEs) and in the case of OLCI, are the cause of isolated across-track pixel stripes present at the L1B imagery where the radiance values appear anomalously high/low with respect to their surroundings. The magnitude and frequency of these stripes are evidently higher in the region of the South Atlantic (Magnetic) Anomaly (SAA), which also covers central South America. In this region, PPE contamination at the top-of-atmosphere (TOA) radiances has a significant impact on water reflectance and biogeophysical product retrieval over the affected pixels, which means they must be detected and removed from the L1B imagery. In this letter, a PPE detection and removal algorithm is proposed to be applied over water bodies, based on a simple moving filter with a 5 x 1 along-track kernel applied over the whole spectral set of OLCI TOA radiances. Its performance was evaluated visually and by comparing with preexistent predictions. Results indicate that images in the SAA region contain 27.8 times more PPE-contaminated pixels than images from outside the SAA and that the most affected bands are at 400 and 1016 nm, where the fraction of PPE-flagged pixels over the SAA reaches 0.14% and 0.26%, respectively.**

***Index Terms*— Atmospheric correction, Ocean and Land Color Instrument (OLCI), turbid waters.**

I. Introduction

THE South Atlantic (Magnetic) Anomaly (SAA) is a feature of the earth's magnetic field that impacts the height of the radiation belts of the planet in the region of central South America and the South Atlantic region adjacent to the coasts of Brazil, Uruguay, and central Argentina. The radiation belt is a region of the earth's space environment where there is a flux of charged particles whose motion follows in a spiral movement about a magnetic field line such that the radius of rotation tends to enclose a constant amount of magnetic flux [11]. Earth's magnetic field is not a geodetically centered dipole, but can be roughly represented (upto first order magnetic moment) by a dipole-shifted northward from the earth's geodetic center, such that the region of the SAA is farthest from its location. This means that every charged particle moving spirally around the magnetic field lines will decrease its altitude to enclose a constant magnetic flux when reaching the SAA region. In other words, the radiation belt that surrounds the earth, defined precisely by the presence of these highly energized electrons and protons with energies in the range 0.001–100 MeV [3], is often found (over the SAA) at altitudes consistent with low earth orbit (LEO) satellites' trajectories [1], such as Sentinel-3 series and EnviSat, whose altitudes are 814.15 [10] and 782 km [2], respectively. Given their specific and similar technological design (thoroughly described in [4]), the charge-coupled devices (CCDs) of the Ocean and Land Color Instrument (OLCI, onboard Sentinel-3) and the MEdium Resolution Imaging Spectrometer (MERIS, onboard EnviSat) are strongly affected by prompt particle event (PPEs) all around the globe, but particularly when the sensor is orbiting inside the SAA. In the case of a PPE, a set of multiple spikes appears in the dark signal, since its level is very low compared to the noise provoked by particles hitting the CCDs, resulting in anomalously low/high derived top-of-atmosphere (TOA) radiances. Due to the fact that the CCD arrays span the along-track spatial dimension and the spectral dimension (each CCD pixel has a size of 22.5 μm corresponds to roughly 300 m $\times$ 1.25 nm), and given that each PPE might affect many adjacent elements, it is expected that the PPE-induced error appears as across-track stripes and along many bands in the L1B data, although the across-track and spectral affected extensions are uncertain and depend on the energy, orientation of the impact, and physical nature of the particles [4]. It has already been studied how these PPEs affect the TOA radiances retrieved by MERIS, and how these events affect product retrieval, such as the case of the maximum chlorophyll index (MCI), which is defined as [8]

$$\mathrm{MCI} = -0.6164.L_{681}^{\mathrm{TOA}} + L_{709}^{\mathrm{TOA}} - 0.3836.L_{754}^{\mathrm{TOA}} \qquad (1)$$

where L_{681}^{TOA} is the TOA radiance at spectral band centered at 681 nm. In the SAA, it has been found that MCI presents a high density of isolated pixels with anomalous values, related to PPEs [8]. This letter is focused on presenting a simple algorithm designed to detect and remove PPE-induced anomalous

Manuscript received March 2, 2018; revised May 8, 2018 and July 11, 2018; accepted September 19, 2018. This work was supported in part by the ANPCyT under Grant PICT 2014-0455, in part by the CONICET under Grant PIP 112 20120100350, in part by the ESA's CASE2X Project under Grant SEOM-DTEX-EOPS-SW-14-0002, and in part by the HYPERMAQ Project through Belgian Science Policy Office in the frame of the STEREO III Program under Grant SR/00/335.

The author is with Instituto de Astronomía y Física del Espacio, CONICET, Universidad de Buenos Aires, Buenos Aires, Argentina (e-mail: gossn@iafe.uba.ar).

Digital Object Identifier 10.1109/LGRS.2018.2872172

1545-598X © 2018 IEEE. Personal use is permitted, but republication/redistribution requires IEEE permission.
See http://www.ieee.org/publications_standards/publications/rights/index.html for more information.

TABLE I

SENSING STARTING TIMES OF IMAGES USED IN THIS LETTER, CORRESPONDING TO REGIONS LABELED "SAA" AND "AUS"

Img. number	SAA	AUS
1	2017-10-07 13:10:14 GMT	2017-10-13 02:02:12 GMT
2	2017-10-15 13:02:45 GMT	2017-10-14 01:36:01 GMT
3	2017-10-16 12:36:34 GMT	2017-10-18 01:32:17 GMT
4	2017-10-19 12:59:00 GMT	2017-10-25 01:50:59 GMT
5	2017-10-30 13:13:58 GMT	2017-10-26 01:24:48 GMT
6	2017-10-31 12:47:47 GMT	2017-10-29 01:47:15 GMT
7	2017-12-24 12:47:47 GMT	2017-11-17 01:54:43 GMT
8	2018-01-04 13:02:45 GMT	2017-11-29 01:43:30 GMT
9	2018-01-08 12:59:01 GMT	2017-11-30 01:17:19 GMT

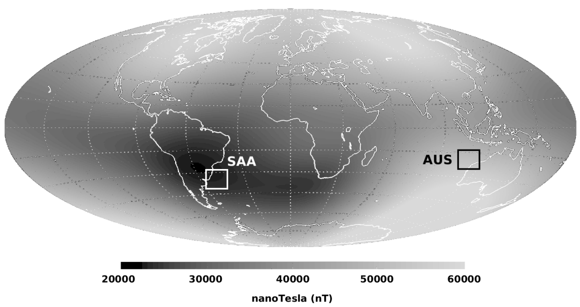

Fig. 1. Geomagnetic total field intensity at the earth's surface acquired with Swarm constellation between January 1, 2014 and June 30, 2014 [5]. White and black boxes indicate the study regions of the present work, off the coast of Argentina, Uruguay, and Brazil (SAA), and off the coast of northwest Australia (AUS), respectively.

values in TOA radiances (i.e., in L1B data) of OLCI and MERIS sensors. The proposed method is based on a pixel-by-pixel 5 × 1 moving along-track kernel applied over each band, and was tested and implemented successfully on OLCI imagery. The performance was evaluated visually and by comparing the fraction of contaminated pixels and the associated TOA radiance error with preexistent predictions [4]. The implementation of this removal over L1B data will reduce contaminated data and retrieval failures in products such as MCI, atmospherically corrected reflectance, among others.

II. STUDY REGION AND IMAGE DATA SET

A total of 18 cloud and land-free subscenes of L1B data (see Table I) from the entire set of OLCI bands were analyzed from regions inside and outside the SAA, to compare the amount and intensity of PPE-contaminated pixels between both sites (called here "SAA" and "AUS" and marked in Fig. 1 as white and black boxes, respectively). The data were downloaded From Copernicus online data access system [6] and correspond to the processing baseline v2.23, which holds for the first reprocessing of OLCI scenes [2]. The SAA selected subregion corresponds to the Atlantic Ocean off the coasts of Argentina, Brazil, and Uruguay, including the Río de la Plata highly turbid river estuary, located between Argentina and Uruguay. In this selected region, the intensity in magnetic field is expected to be minimum (∼19000 nT at an altitude of 614 km). The other region, called here "AUS" corresponds to the Indian Ocean off the coast of north west Australia, where there is simultaneously a relatively high magnetic field and a relatively low average cloud cover [7].

The development, testing, and implementation of the algorithm was performed on OLCI L1B products, i.e., over TOA radiance imagery following the detection geometry of the CCD pixels (see Figs. 2 and 3). This means that rows and columns in L1B TOA radiances correspond to the across- and along-track sensing directions, respectively.

Two complementary reasons were considered to implement the algorithm in this geometry: 1) the PPE-induced noise is oriented across track and 2) the potential camera boundary artifacts are oriented along track, together with other artifacts such as fixed pattern noise [4]. This means that in this geometry, PPEs are easily identifiable as across-track stripes and orthogonal with respect to eventual along-track camera effects.

III. DETECTION AND REMOVAL ALGORITHM

The detection of PPE-contaminated pixels on L1B imagery was applied over each OLCI band separately in a pixel-by-pixel basis. The scheme is summarized as follows (see Fig. 4).

1) For a given pixel located at (r, c) (i.e., at row r and column c), a 5 × 1 along track kernel is considered, i.e., taking also into account the group of neighbor pixels at (r', c), being $r' = r-2, r-1, r+1, r+2$.
2) The median and median absolute deviation (MAD) of TOA radiances at the pixels in (r', c) of $L^{\text{TOA}}_{r',c}$ are computed [$\text{mdn}(L^{\text{TOA}}_{r',c})$ and $\text{MAD}(L^{\text{TOA}}_{r',c})$, respectively)] The MAD is defined as
$$\text{MAD}\big(L^{\text{TOA}}_{r',c}\big) = \text{mdn}\big(\big|L^{\text{TOA}}_{r',c} - \text{mdn}(L^{\text{TOA}}_{r',c})\big|\big). \quad (2)$$
3) If the TOA radiance value at (r, c) differs from the computed median by more than ten times the computed MAD, and also differs by more than a minimum threshold of 0.7 mW/nm/sr/m^2, then the PPE flag is set to true. Mathematically, the condition can be expressed as follows:
$$\big|L^{\text{TOA}}_{r,c} - \text{mdn}\big(L^{\text{TOA}}_{r',c}\big)\big| > \max\,\big\{10.\text{MAD}\big(L^{\text{TOA}}_{r',c}\big); 0.7\big\}. \quad (3)$$
4) If the PPE flag is true, then the affected TOA radiance value at pixel (r, c) is replaced by the median of the (r', c) set, i.e., $L^{\text{TOA}}_{r,c} \rightarrow \text{mdn}(L^{\text{TOA}}_{r',c})$. The PPE flag could then be propagated to level 2 data to notify users that a "replacement value" has been used.

The algorithm looks at the four nearest along-track neighbors instead of 2 because the across-track stripes produced by PPE contamination might take more than one row in exceptional cases (upto three rows). Also it uses median (mdn) and MAD as measures of central value and dispersion as more robust statistics with respect to outliers compared to usual statistics such as mean and standard deviation. These outliers might be produced, in the cases of high PPE contamination, by other PPEs affecting the (r', c) pixels. This occurs only in exceptional cases inside the SAA and in highly contaminated bands (such as 400 and 1016 nm). The 10 factor applied to the MAD term was determined from visual inspection of cloudy scenes where, given smaller factors than 10, small clouds were incorrectly detected as PPEs. Finally, the minimum threshold radiance of 0.7 mW/nm/sr/m^2 was set to avoid false

IEEE Proof

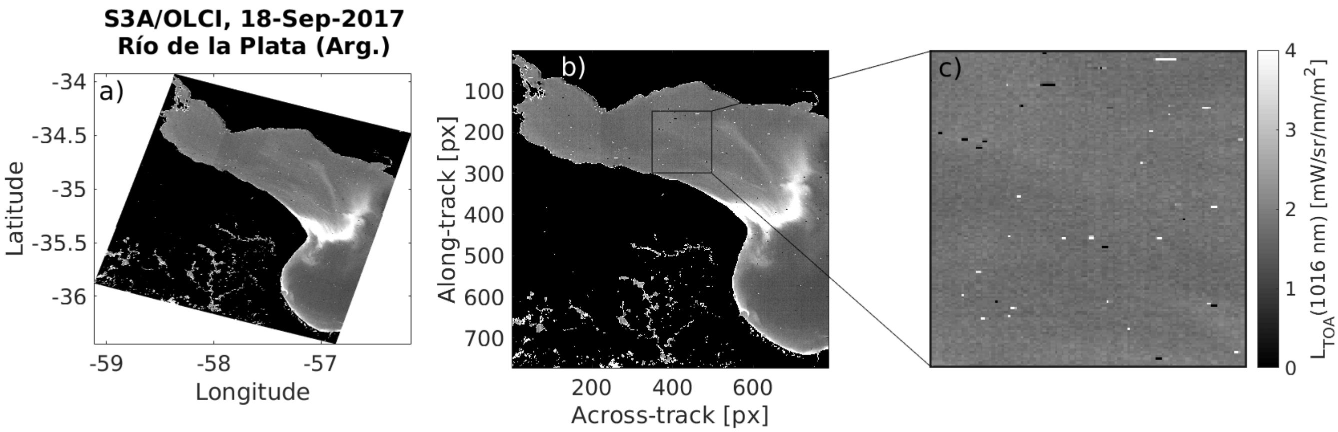

Fig. 2. TOA radiance at 1016 nm, taken by OLCI over the Río de la Plata river inside the SAA region (acquisition date: September 18, 2017, 13:02:45 GMT), where the presence of PPEs is observed as isolated pixel stripes with extremely high or low radiance. (a) Plate-carre projection, (b) row-column geometry (as in L1B data), where PPE-contaminated pixel stripes are across-track, and (c) zoomed-in-view at smaller subregion to better visualize the contaminated pixels.

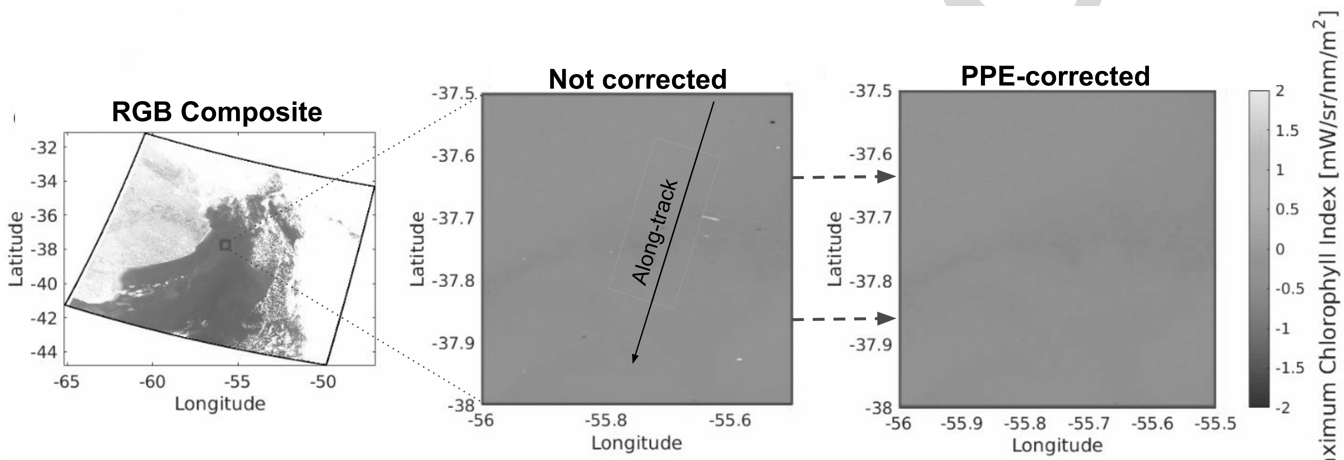

(a) (b) (c)

Fig. 3. MCI false alarms reported by Gower *et al.* [9] might be markedly reduced by applying the PPE removal algorithm proposed in this letter. (a) RGB composite of image from the SAA set (October 19, 2017, 12:59:00 GMT), corresponding to the Argentinean Sea. (b) MCI computed in a $0.5° \times 0.5°$ box subset, [using (1)], where the the impact of PPEs is easily recognizable as extremely low/high MCI values in isolated pixel stripes, orthogonal to the along-track direction. (c) MCI computed in a $0.5° \times 0.5°$ box subset but after PPE-removal.

PPE flags where the variability in (r', c) pixels, quantified through $\mathrm{MAD}(L^{\mathrm{TOA}}_{r',c})$, is anomalously small; and also has to do with the nature of the PPE-induced error in TOA radiance: D'Amico *et al.* [4] predicted that, given a pixel is contaminated by a PPE, the probability density function over the expected TOA radiance absolute error is expected to follow a simple exponential decay law with e-folding scale of 1 and initial step of 0.81 mW/nm/sr/m^2 [this means null probability of being smaller than 0.81 mW/nm/sr/m^2, see Fig. 6(f)]. The smaller threshold of 0.7 mW/nm/sr/m^2 was set to account for exceptional cases where the PPE induced error is slightly smaller than 0.81 mW/nm/sr/m^2.

It must be mentioned that generally small clouds, islands or any other natural source of variability do not follow the special PPE across-track orientation, but exceptionally could affect solitary lines. In the exceptional cases of small islands, these should be detected by preexistent land masks, and it is not the scope of this algorithm to detect them. The 10.MAD term usually avoids small clouds from being detected as PPEs, but also preexistent cloud masking should not be confounding clouds and PPEs given that clouds are nearly spectrally white, while PPEs in general are not white. In the cases of coastlines, turbidity plumes or other sources of natural variability, the observed spatial variations are smoother (than PPEs) and/or the difference in radiance values inside each along-track kernel is not high enough to be detected as PPEs.

IV. Results and Discussion

Fig. 5 shows an example of how the PPE removal works for two subscenes, one inside the SAA box (October 19, 2017 12:59:00 GMT) and one inside the AUS box (October 25, 2017 01:50:59 GMT) (SAA and AUS boxes are shown in Fig. 1). The 1016 nm band (Oa_21) was chosen to illustrate the PPE removal, since it is the most affected of all 21 OLCI bands (see Fig. 6). This shows how PPEs occur more often in the SAA region than in other sites where the magnetic field intensity is higher.

Fig. 6 shows the percentages of PPE-flagged pixels of the selected study regions SAA and AUS for each of the 21 bands on OLCI. The two sets were composed of 9 land and cloud-free one-squared-degree from the period September 2017–January 2018. The reported fractions are

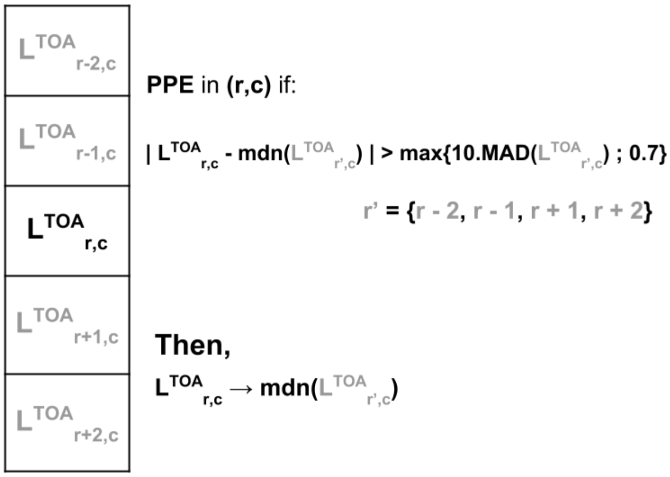

Fig. 4. Scheme describing the PPE detection algorithm for a given pixel located at (r, c), by comparing its TOA radiance with the radiances at its nearest four along-track neighbors [called here (r', c)].

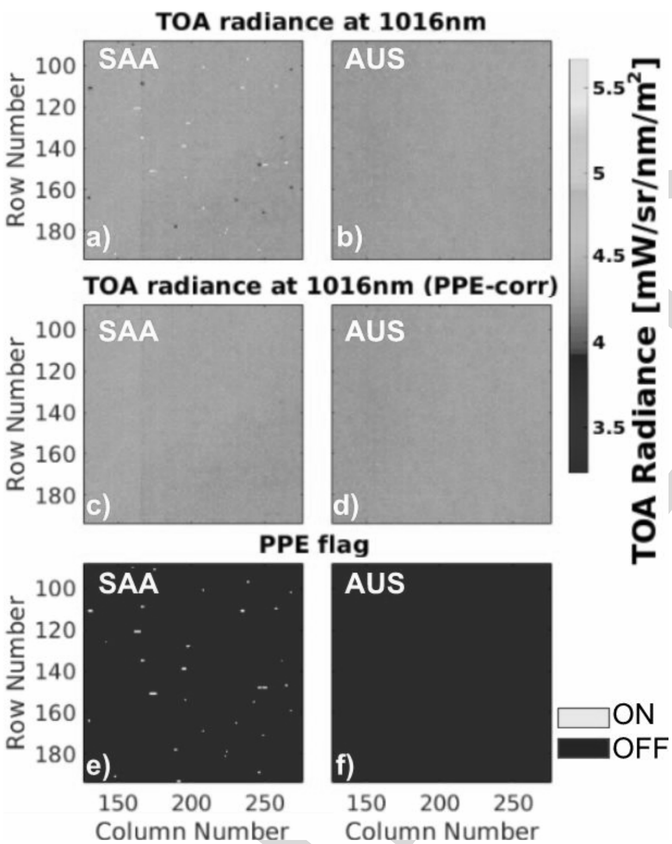

Fig. 5. Effect of the PPE-removal scheme over the TOA radiance at 1016 nm for regions (Left) SAA and (Right) AUS. (a) and (b) TOA radiances at 1016 nm. (c) and (d) TOA radiances at 1016 nm but corrected for PPEs (where flagged pixels were corrected as described in Section III, Fig. 4). (e) and (f) PPE-flagged pixels are shown in light gray.

calculated as the total number of PPE-flagged pixels divided by the total pixels from the nine subsets considered for each region. It is clearly observable from Fig. 6 how the SAA region is more affected by PPE events than AUS, which is certainly more "magnetically shielded," which means that PPEs are highly unlikely in comparison. A larger percent of PPE-flagged pixels is observed for SAA set at bands 400 (median, 0.14%)

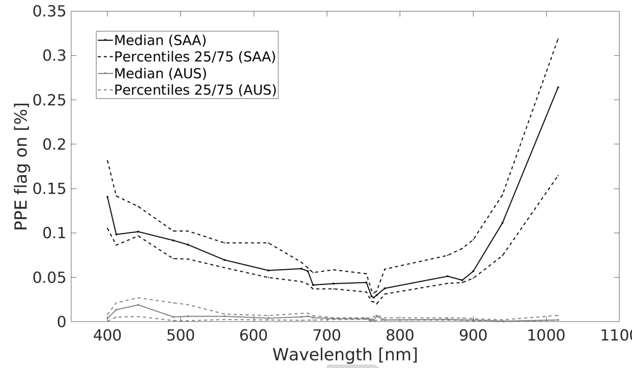

Fig. 6. Percentage of pixels flagged as PPE contaminated, evaluated over a set of 18 subsets of 1 squared degree, 9 from each region, SAA (black curves) and AUS (gray curves). The amount of affected pixels is on average 27.8 times larger in the SAA region, although the difference is higher at the spectral extremes [Oa_01 (400 nm) and Oa_21 (1016 nm) bands].

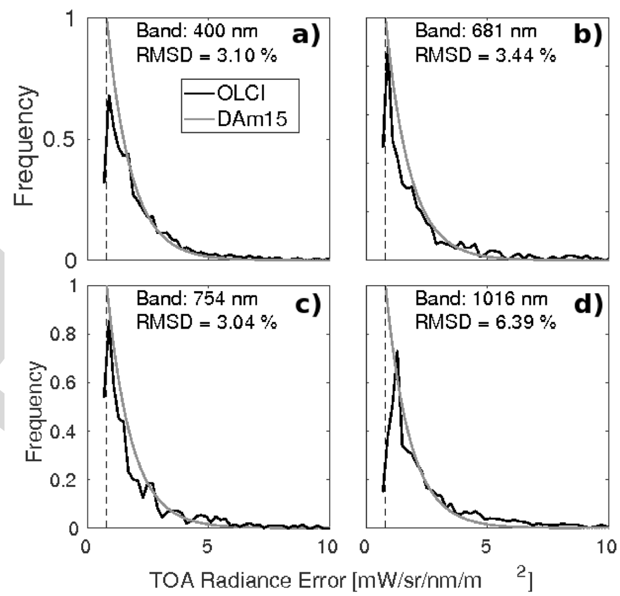

Fig. 7. Conditional probability density distribution of absolute TOA radiance error, given PPE contamination, $p(|L^{\mathrm{TOA}}_{r,c} - \mathrm{mdn}(L^{\mathrm{TOA}}_{r',c})||\mathrm{PPE})$, for bands (a) 400, (b) 681, (c) 709, and (d) 1016 nm. In black, values obtained over OLCI imagery of the "SAA" subset by applying the PPE algorithm. In light gray, predicted distribution by D'Amico *et al.* [4], together with a dashed vertical line at 0.81 mW/nm/sr/m^2, indicating the minimum error expected.

and 1016 nm (median, 0.26%), which is similar to what was observed for MERIS along Envisat descendant orbit 292 in D'Amico *et al.* [4]. The reasons why these bands are more affected by PPEs are related to: 1) more elementary rows assigned inside the CCD and 2) nearness to the aluminum shield of the sensor. In all bands, it is observed at least a 10 times larger fraction of PPE-flagged pixels in the SAA region with respect to the AUS region.

Other interesting quantity to analyze is the absolute correction applied over the PPE-flagged pixels, i.e., the distribution of $|L^{\mathrm{TOA}}_{r,c} - \mathrm{mdn}(L^{\mathrm{TOA}}_{r',c})|$, given a pixel was PPE-flagged [see (3)]. Fig. 7 shows the normalized histograms of $|L^{\mathrm{TOA}}_{r,c} - \mathrm{mdn}(L^{\mathrm{TOA}}_{r',c})|$ for PPE-flagged pixels (labeled as TOA radiance error) for the bands (a) 400 nm, (b) 681 nm, (c) 754 nm, and (d) 1016 nm. In all cases, the histograms resemble the shifted exponential decay predicted in [4, Fig. 6.3.2].

As an example of how PPEs might affect product retrieval, Fig. 3 shows an MCI map, calculated using (1). Gower *et al.* [9] already ascertained that a high amount of isolated MCI false alarms were produced in the region affected by the SAA, and they attributed this phenomenon to PPEs. What is shown in Fig. 3 clearly endorses this assertion, as in the uncorrected subscene [Fig. 3(b)], isolated across-track stripes of probably unnatural extremely low/high MCI values are observed (upto 15 mW/nm/sr/m^2 in the worse cases). After the PPE removal scheme, these isolated extreme values tend to be smoothed out, as shown in Fig. 3(c). This same behavior is observed throughout the entire set of selected images from the SAA region.

V. Conclusion

In this letter, a scheme for detection and removal of PPEs from L1B OLCI ocean color images is proposed. It is based on a pixel-by-pixel moving along-track 5×1 kernel and it is applied to all bands. As predicted, it was observed that PPEs affect on average 27.8 times more pixels inside the SAA than in other geographical regions. The absolute errors in TOA radiances induced by PPEs follow a similar pattern to that predicted by D'Amico *et al.* [4], i.e., a shifted exponential decay probability density function, of e-folding of 1 and initial shift of 0.81 mW/nm/sr/m^2 [4]. As an example of how PPEs might induce product retrieval failure, Gower *et al.* [9] alerted for the presence of anomalous isolated MCI alarms, especially in the region the SAA. It is shown how these false isolated alarms will be markedly reduced by applying the PPE-removal scheme over L1B imagery. Despite the fact that PPEs are highly unlikely outside the SAA region, the probability of occurrence are not reduced to zero. Taking this into account and the fact that the geomagnetic field is not stationary, it is recommended to apply the described PPE-removal scheme over all the L1B imagery, and not just over the South Atlantic region. The proposed algorithm can be easily extended to other PPE-sensitive sensors flying on LOEs.

Acknowledgment

The author would like to thank K. G. Ruddick, A. I. Dogliotti, F. M. Grings, J. Nieke, F. D'Amico, and two anonymous reviewers for very helpful comments.

References

[1] G. D. Badhwar, V. V. Kushin, Y. A. Akatov, and V. A. Myltseva, "Effects of trapped proton flux anisotropy on dose rates in low Earth orbit," *Radiat. Meas.*, vol. 30, no. 3, pp. 415–426, Jun. 1999.

[2] Sentinels. *Copernicus*. Accessed: Feb. 14, 2018. [Online]. Available: https://sentinels.copernicus.eu

[3] T. E. Cravens, *Physics of Solar System Plasmas*. Cambridge, U.K.: Cambridge Univ. Press, 1997.

[4] F. D'Amico, G. Corsini, M. Diani, and J. Nieke, "Prompt-particle-events in ESA's Envisat/MERIS and Sentinel-3/OLCI data: Observations, analysis and recommendations," M.S. thesis, Dipartimento Ingegneria dell'Informazione, Univ. Pisa, Pisa, Italy, 2015.

[5] *NASA's Earth Observatory*. Accessed: Feb. 22, 2018. [Online]. Available: https://earthobservatory.nasa.gov/IOTD/view.php?id=84266

[6] EUMETSAT Official Website. *Copernicus Online Data Access*. Accessed: Feb. 3, 2018. [Online]. Available: https://eumetsat.int/website/home/Data/DataDelivery/CopernicusOnlineDataAccess/index.html

[7] ESA Official Website. (2014). *European Space Agency*. [Online]. Available: https://esa.int/spaceinimages/Images/2013/09/Cloud_cover_Thales_Alenia_Space

[8] J. F. R. Gower, C. Hu, G. A. Borstad, and S. King, "Ocean color satellites show extensive lines of floating Sargassum in the Gulf of Mexico," *IEEE Trans. Geosci. Remote Sens.*, vol. 44, pp. 3619–3625, 2006.

[9] J. Gower, S. King, and P. Goncalves, "Global monitoring of plankton blooms using MERIS MCI," *Int. J. Remote Sens.*, vol. 29, no. 21, pp. 6209–6216, 2008, doi: 10.1080/01431160802178110.

[10] J. Nieke *et al.*, "Ocean and land colour imager on Sentinel-3," in *Optical Payloads for Space Missions*, S.-E. Qian, Ed. Hoboken, NJ, USA: Wiley, ch. 10, pp. 223–245.

[11] P. A. Sturrock, J. A. Klimchuk, G. Roumeliotis, and S. K. Antiochos, "The asymptotic behavior of force-free magnetic-field configurations," in *Proc. 14th Int. Summer Workshop, Nat. Sol. Observatory*, vol. 68, Sunspot, NM, USA, Aug./Sep. 1993, pp. 219–224.

IEEE Proof

Effect of Prompt Particle Events on OLCI Ocean Color Imagery in the South Atlantic Anomaly: Detection and Removal

Juan I. Gossn

***Abstract*— It has been found that cosmic rays and massive charged particles trapped in the magnetosphere or arriving from the sun might produce spike noise over the dark offset signal coming from charge-coupled devices (CCDs) on optic sensors such as Ocean and Land Color Instrument (Sentinel-3/OLCI) and Medium Resolution Imaging Spectrometer (Envisat/MERIS). These phenomena are called prompt particle events (PPEs) and in the case of OLCI, are the cause of isolated across-track pixel stripes present at the L1B imagery where the radiance values appear anomalously high/low with respect to their surroundings. The magnitude and frequency of these stripes are evidently higher in the region of the South Atlantic (Magnetic) Anomaly (SAA), which also covers central South America. In this region, PPE contamination at the top-of-atmosphere (TOA) radiances has a significant impact on water reflectance and biogeophysical product retrieval over the affected pixels, which means they must be detected and removed from the L1B imagery. In this letter, a PPE detection and removal algorithm is proposed to be applied over water bodies, based on a simple moving filter with a 5 x 1 along-track kernel applied over the whole spectral set of OLCI TOA radiances. Its performance was evaluated visually and by comparing with preexistent predictions. Results indicate that images in the SAA region contain 27.8 times more PPE-contaminated pixels than images from outside the SAA and that the most affected bands are at 400 and 1016 nm, where the fraction of PPE-flagged pixels over the SAA reaches 0.14% and 0.26%, respectively.**

***Index Terms*— Atmospheric correction, Ocean and Land Color Instrument (OLCI), turbid waters.**

I. Introduction

The South Atlantic (Magnetic) Anomaly (SAA) is a feature of the earth's magnetic field that impacts the height of the radiation belts of the planet in the region of central South America and the South Atlantic region adjacent to the coasts of Brazil, Uruguay, and central Argentina. The radiation belt is a region of the earth's space environment where there is a flux of charged particles whose motion follows in a spiral movement about a magnetic field line such that the radius of rotation tends to enclose a constant amount of magnetic flux [11]. Earth's magnetic field is not a geodetically centered dipole, but can be roughly represented (upto first order magnetic moment) by a dipole-shifted northward from the earth's geodetic center, such that the region of the SAA is farthest from its location. This means that every charged particle moving spirally around the magnetic field lines will decrease its altitude to enclose a constant magnetic flux when reaching the SAA region. In other words, the radiation belt that surrounds the earth, defined precisely by the presence of these highly energized electrons and protons with energies in the range 0.001–100 MeV [3], is often found (over the SAA) at altitudes consistent with low earth orbit (LEO) satellites' trajectories [1], such as Sentinel-3 series and EnviSat, whose altitudes are 814.15 [10] and 782 km [2], respectively. Given their specific and similar technological design (thoroughly described in [4]), the charge-coupled devices (CCDs) of the Ocean and Land Color Instrument (OLCI, onboard Sentinel-3) and the MEdium Resolution Imaging Spectrometer (MERIS, onboard EnviSat) are strongly affected by prompt particle event (PPEs) all around the globe, but particularly when the sensor is orbiting inside the SAA. In the case of a PPE, a set of multiple spikes appears in the dark signal, since its level is very low compared to the noise provoked by particles hitting the CCDs, resulting in anomalously low/high derived top-of-atmosphere (TOA) radiances. Due to the fact that the CCD arrays span the along-track spatial dimension and the spectral dimension (each CCD pixel has a size of 22.5 μm corresponds to roughly 300 m $\times$ 1.25 nm), and given that each PPE might affect many adjacent elements, it is expected that the PPE-induced error appears as across-track stripes and along many bands in the L1B data, although the across-track and spectral affected extensions are uncertain and depend on the energy, orientation of the impact, and physical nature of the particles [4]. It has already been studied how these PPEs affect the TOA radiances retrieved by MERIS, and how these events affect product retrieval, such as the case of the maximum chlorophyll index (MCI), which is defined as [8]

$$\mathrm{MCI} = -0.6164.L_{681}^{\mathrm{TOA}} + L_{709}^{\mathrm{TOA}} - 0.3836.L_{754}^{\mathrm{TOA}} \quad (1)$$

where L_{681}^{TOA} is the TOA radiance at spectral band centered at 681 nm. In the SAA, it has been found that MCI presents a high density of isolated pixels with anomalous values, related to PPEs [8]. This letter is focused on presenting a simple algorithm designed to detect and remove PPE-induced anomalous

Manuscript received March 2, 2018; revised May 8, 2018 and July 11, 2018; accepted September 19, 2018. This work was supported in part by the ANPCyT under Grant PICT 2014-0455, in part by the CONICET under Grant PIP 112 20120100350, in part by the ESA's CASE2X Project under Grant SEOM-DTEX-EOPS-SW-14-0002, and in part by the HYPERMAQ Project through Belgian Science Policy Office in the frame of the STEREO III Program under Grant SR/00/335.

The author is with Instituto de Astronomía y Física del Espacio, CONICET, Universidad de Buenos Aires, Buenos Aires, Argentina (e-mail: gossn@iafe.uba.ar).

Digital Object Identifier 10.1109/LGRS.2018.2872172

1545-598X © 2018 IEEE. Personal use is permitted, but republication/redistribution requires IEEE permission.
See http://www.ieee.org/publications_standards/publications/rights/index.html for more information.

IEEE Proof

TABLE I

SENSING STARTING TIMES OF IMAGES USED IN THIS LETTER, CORRESPONDING TO REGIONS LABELED "SAA" AND "AUS"

Img. number	SAA	AUS
1	2017-10-07 13:10:14 GMT	2017-10-13 02:02:12 GMT
2	2017-10-15 13:02:45 GMT	2017-10-14 01:36:01 GMT
3	2017-10-16 12:36:34 GMT	2017-10-18 01:32:17 GMT
4	2017-10-19 12:59:00 GMT	2017-10-25 01:50:59 GMT
5	2017-10-30 13:13:58 GMT	2017-10-26 01:24:48 GMT
6	2017-10-31 12:47:47 GMT	2017-10-29 01:47:15 GMT
7	2017-12-24 12:47:47 GMT	2017-11-17 01:54:43 GMT
8	2018-01-04 13:02:45 GMT	2017-11-29 01:43:30 GMT
9	2018-01-08 12:59:01 GMT	2017-11-30 01:17:19 GMT

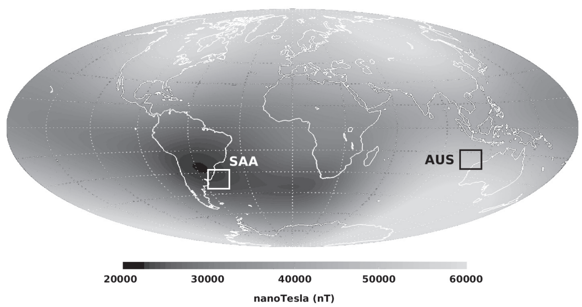

Fig. 1. Geomagnetic total field intensity at the earth's surface acquired with Swarm constellation between January 1, 2014 and June 30, 2014 [5]. White and black boxes indicate the study regions of the present work, off the coast of Argentina, Uruguay, and Brazil (SAA), and off the coast of northwest Australia (AUS), respectively.

values in TOA radiances (i.e., in L1B data) of OLCI and MERIS sensors. The proposed method is based on a pixel-by-pixel 5×1 moving along-track kernel applied over each band, and was tested and implemented successfully on OLCI imagery. The performance was evaluated visually and by comparing the fraction of contaminated pixels and the associated TOA radiance error with preexistent predictions [4]. The implementation of this removal over L1B data will reduce contaminated data and retrieval failures in products such as MCI, atmospherically corrected reflectance, among others.

II. STUDY REGION AND IMAGE DATA SET

A total of 18 cloud and land-free subscenes of L1B data (see Table I) from the entire set of OLCI bands were analyzed from regions inside and outside the SAA, to compare the amount and intensity of PPE-contaminated pixels between both sites (called here "SAA" and "AUS" and marked in Fig. 1 as white and black boxes, respectively). The data were downloaded From Copernicus online data access system [6] and correspond to the processing baseline v2.23, which holds for the first reprocessing of OLCI scenes [2]. The SAA selected subregion corresponds to the Atlantic Ocean off the coasts of Argentina, Brazil, and Uruguay, including the Río de la Plata highly turbid river estuary, located between Argentina and Uruguay. In this selected region, the intensity in magnetic field is expected to be minimum (∼19000 nT at an altitude of 614 km). The other region, called here "AUS" corresponds to the Indian Ocean off the coast of north west Australia, where there is simultaneously a relatively high magnetic field and a relatively low average cloud cover [7].

The development, testing, and implementation of the algorithm was performed on OLCI L1B products, i.e., over TOA radiance imagery following the detection geometry of the CCD pixels (see Figs. 2 and 3). This means that rows and columns in L1B TOA radiances correspond to the across- and along-track sensing directions, respectively.

Two complementary reasons were considered to implement the algorithm in this geometry: 1) the PPE-induced noise is oriented across track and 2) the potential camera boundary artifacts are oriented along track, together with other artifacts such as fixed pattern noise [4]. This means that in this geometry, PPEs are easily identifiable as across-track stripes and orthogonal with respect to eventual along-track camera effects.

III. DETECTION AND REMOVAL ALGORITHM

The detection of PPE-contaminated pixels on L1B imagery was applied over each OLCI band separately in a pixel-by-pixel basis. The scheme is summarized as follows (see Fig. 4).

1) For a given pixel located at (r, c) (i.e., at row r and column c), a 5×1 along track kernel is considered, i.e., taking also into account the group of neighbor pixels at (r', c), being $r' = r-2, r-1, r+1, r+2$.
2) The median and median absolute deviation (MAD) of TOA radiances at the pixels in (r', c) of $L^{\text{TOA}}_{r',c}$ are computed [$\text{mdn}(L^{\text{TOA}}_{r',c})$ and $\text{MAD}(L^{\text{TOA}}_{r',c})$, respectively)] The MAD is defined as

$$\text{MAD}\big(L^{\text{TOA}}_{r',c}\big) = \text{mdn}\big(\big|L^{\text{TOA}}_{r',c} - \text{mdn}(L^{\text{TOA}}_{r',c})\big|\big). \quad (2)$$

3) If the TOA radiance value at (r, c) differs from the computed median by more than ten times the computed MAD, and also differs by more than a minimum threshold of 0.7 mW/nm/sr/m^2, then the PPE flag is set to true. Mathematically, the condition can be expressed as follows:

$$\big|L^{\text{TOA}}_{r,c} - \text{mdn}\big(L^{\text{TOA}}_{r',c}\big)\big| > \max\big\{10.\text{MAD}\big(L^{\text{TOA}}_{r',c}\big); 0.7\big\}. \quad (3)$$

4) If the PPE flag is true, then the affected TOA radiance value at pixel (r, c) is replaced by the median of the (r', c) set, i.e., $L^{\text{TOA}}_{r,c} \rightarrow \text{mdn}(L^{\text{TOA}}_{r',c})$. The PPE flag could then be propagated to level 2 data to notify users that a "replacement value" has been used.

The algorithm looks at the four nearest along-track neighbors instead of 2 because the across-track stripes produced by PPE contamination might take more than one row in exceptional cases (upto three rows). Also it uses median (mdn) and MAD as measures of central value and dispersion as more robust statistics with respect to outliers compared to usual statistics such as mean and standard deviation. These outliers might be produced, in the cases of high PPE contamination, by other PPEs affecting the (r', c) pixels. This occurs only in exceptional cases inside the SAA and in highly contaminated bands (such as 400 and 1016 nm). The 10 factor applied to the MAD term was determined from visual inspection of cloudy scenes where, given smaller factors than 10, small clouds were incorrectly detected as PPEs. Finally, the minimum threshold radiance of 0.7 mW/nm/sr/m^2 was set to avoid false

IEEE Proof

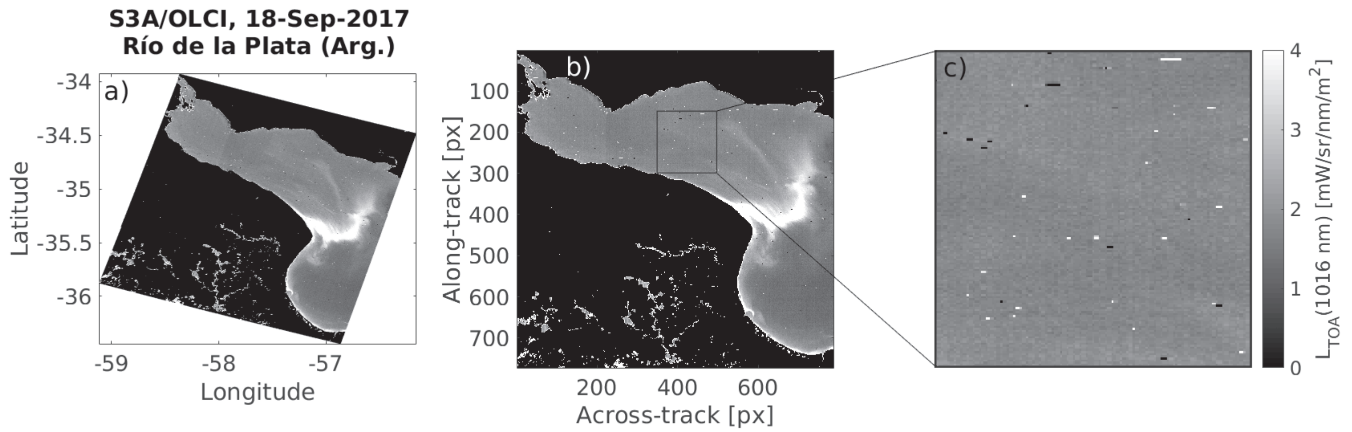

Fig. 2. TOA radiance at 1016 nm, taken by OLCI over the Río de la Plata river inside the SAA region (acquisition date: September 18, 2017, 13:02:45 GMT), where the presence of PPEs is observed as isolated pixel stripes with extremely high or low radiance. (a) Plate-carre projection, (b) row-column geometry (as in L1B data), where PPE-contaminated pixel stripes are across-track, and (c) zoomed-in-view at smaller subregion to better visualize the contaminated pixels.

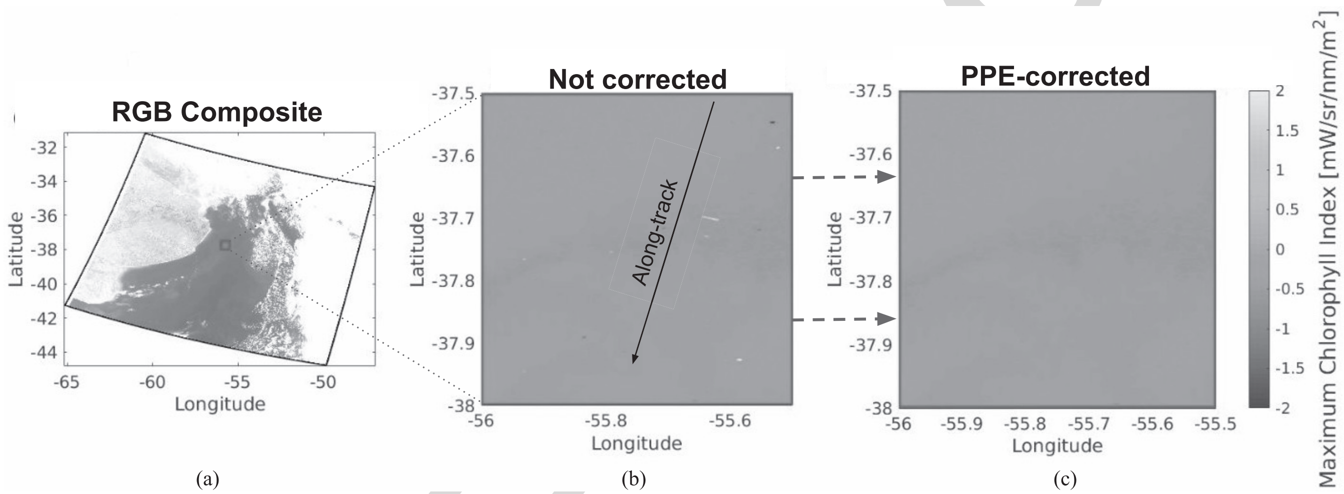

Fig. 3. MCI false alarms reported by Gower *et al.* [9] might be markedly reduced by applying the PPE removal algorithm proposed in this letter. (a) RGB composite of image from the SAA set (October 19, 2017, 12:59:00 GMT), corresponding to the Argentinean Sea. (b) MCI computed in a $0.5^\circ \times 0.5^\circ$ box subset, [using (1)], where the the impact of PPEs is easily recognizable as extremely low/high MCI values in isolated pixel stripes, orthogonal to the along-track direction. (c) MCI computed in a $0.5^\circ \times 0.5^\circ$ box subset but after PPE-removal.

PPE flags where the variability in (r', c) pixels, quantified through $\mathrm{MAD}(L^{\mathrm{TOA}}_{r',c})$, is anomalously small; and also has to do with the nature of the PPE-induced error in TOA radiance: D'Amico *et al.* [4] predicted that, given a pixel is contaminated by a PPE, the probability density function over the expected TOA radiance absolute error is expected to follow a simple exponential decay law with e-folding scale of 1 and initial step of 0.81 mW/nm/sr/m^2 [this means null probability of being smaller than 0.81 mW/nm/sr/m^2, see Fig. 6(f)]. The smaller threshold of 0.7 mW/nm/sr/m^2 was set to account for exceptional cases where the PPE induced error is slightly smaller than 0.81 mW/nm/sr/m^2.

It must be mentioned that generally small clouds, islands or any other natural source of variability do not follow the special PPE across-track orientation, but exceptionally could affect solitary lines. In the exceptional cases of small islands, these should be detected by preexistent land masks, and it is not the scope of this algorithm to detect them. The 10.MAD term usually avoids small clouds from being detected as PPEs, but also preexistent cloud masking should not be confounding clouds and PPEs given that clouds are nearly spectrally white, while PPEs in general are not white. In the cases of coastlines, turbidity plumes or other sources of natural variability, the observed spatial variations are smoother (than PPEs) and/or the difference in radiance values inside each along-track kernel is not high enough to be detected as PPEs.

IV. Results and Discussion

Fig. 5 shows an example of how the PPE removal works for two subscenes, one inside the SAA box (October 19, 2017 12:59:00 GMT) and one inside the AUS box (October 25, 2017 01:50:59 GMT) (SAA and AUS boxes are shown in Fig. 1). The 1016 nm band (Oa_21) was chosen to illustrate the PPE removal, since it is the most affected of all 21 OLCI bands (see Fig. 6). This shows how PPEs occur more often in the SAA region than in other sites where the magnetic field intensity is higher.

Fig. 6 shows the percentages of PPE-flagged pixels of the selected study regions SAA and AUS for each of the 21 bands on OLCI. The two sets were composed of 9 land and cloud-free one-squared-degree from the period September 2017–January 2018. The reported fractions are

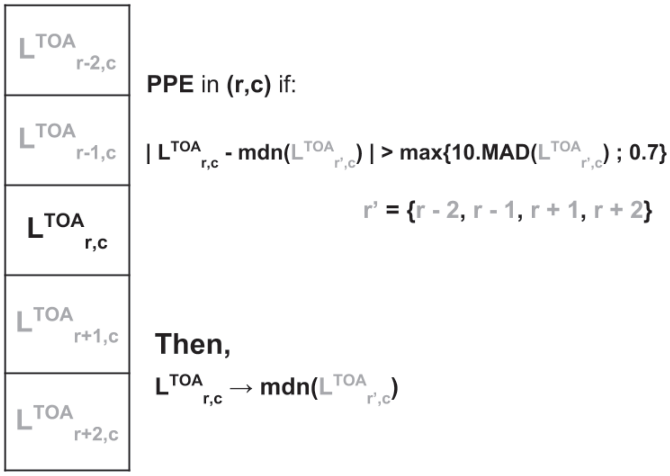

Fig. 4. Scheme describing the PPE detection algorithm for a given pixel located at (r, c), by comparing its TOA radiance with the radiances at its nearest four along-track neighbors [called here (r', c)].

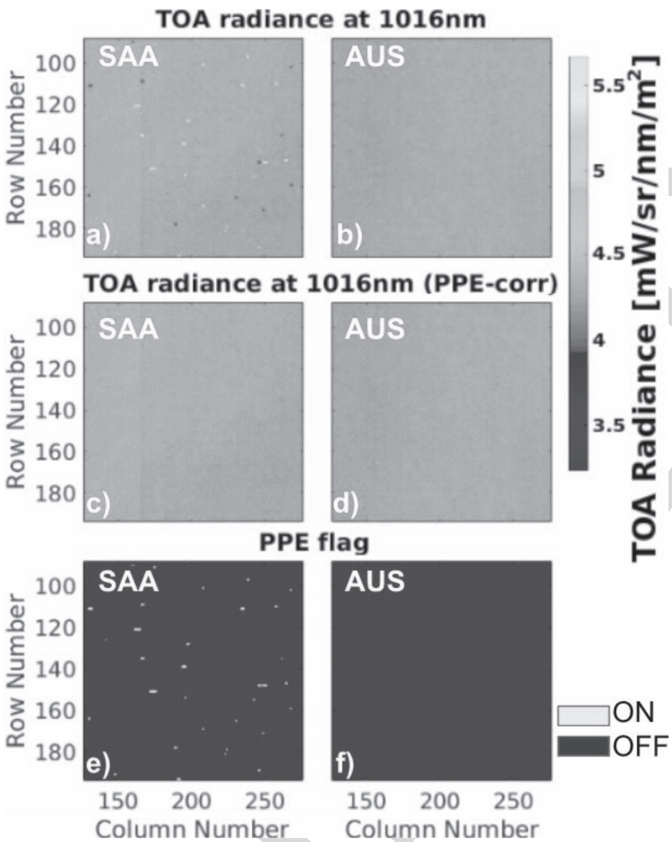

Fig. 5. Effect of the PPE-removal scheme over the TOA radiance at 1016 nm for regions (Left) SAA and (Right) AUS. (a) and (b) TOA radiances at 1016 nm. (c) and (d) TOA radiances at 1016 nm but corrected for PPEs (where flagged pixels were corrected as described in Section III, Fig. 4). (e) and (f) PPE-flagged pixels are shown in light gray.

calculated as the total number of PPE-flagged pixels divided by the total pixels from the nine subsets considered for each region. It is clearly observable from Fig. 6 how the SAA region is more affected by PPE events than AUS, which is certainly more "magnetically shielded," which means that PPEs are highly unlikely in comparison. A larger percent of PPE-flagged pixels is observed for SAA set at bands 400 (median, 0.14%)

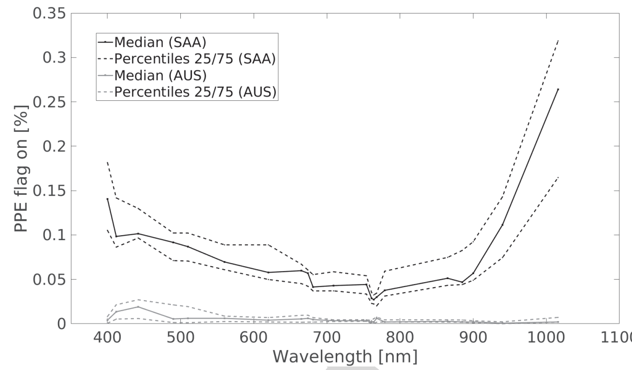

Fig. 6. Percentage of pixels flagged as PPE contaminated, evaluated over a set of 18 subsets of 1 squared degree, 9 from each region, SAA (black curves) and AUS (gray curves). The amount of affected pixels is on average 27.8 times larger in the SAA region, although the difference is higher at the spectral extremes [Oa_01 (400 nm) and Oa_21 (1016 nm) bands].

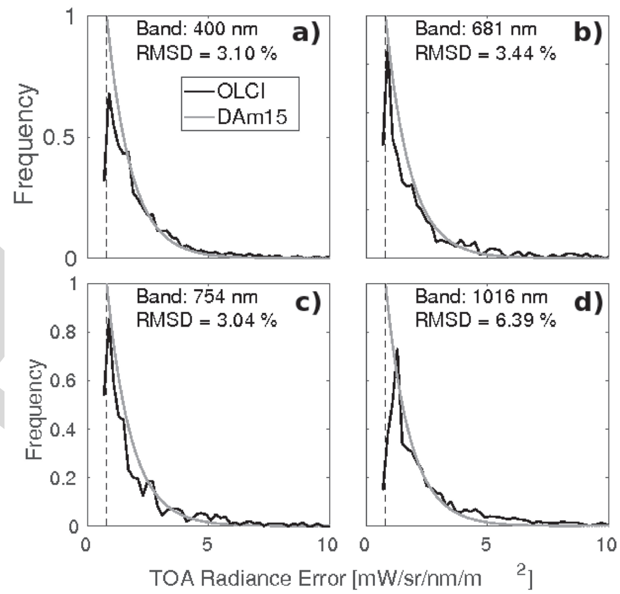

Fig. 7. Conditional probability density distribution of absolute TOA radiance error, given PPE contamination, $p(|L^{\mathrm{TOA}}_{r,c} - \mathrm{mdn}(L^{\mathrm{TOA}}_{r',c})||\mathrm{PPE})$, for bands (a) 400, (b) 681, (c) 709, and (d) 1016 nm. In black, values obtained over OLCI imagery of the "SAA" subset by applying the PPE algorithm. In light gray, predicted distribution by D'Amico *et al.* [4], together with a dashed vertical line at 0.81 mW/nm/sr/m^2, indicating the minimum error expected.

and 1016 nm (median, 0.26%), which is similar to what was observed for MERIS along Envisat descendant orbit 292 in D'Amico *et al.* [4]. The reasons why these bands are more affected by PPEs are related to: 1) more elementary rows assigned inside the CCD and 2) nearness to the aluminum shield of the sensor. In all bands, it is observed at least a 10 times larger fraction of PPE-flagged pixels in the SAA region with respect to the AUS region.

Other interesting quantity to analyze is the absolute correction applied over the PPE-flagged pixels, i.e., the distribution of $|L^{\mathrm{TOA}}_{r,c} - \mathrm{mdn}(L^{\mathrm{TOA}}_{r',c})|$, given a pixel was PPE-flagged [see (3)]. Fig. 7 shows the normalized histograms of $|L^{\mathrm{TOA}}_{r,c} - \mathrm{mdn}(L^{\mathrm{TOA}}_{r',c})|$ for PPE-flagged pixels (labeled as TOA radiance error) for the bands (a) 400 nm, (b) 681 nm, (c) 754 nm, and (d) 1016 nm. In all cases, the histograms resemble the shifted exponential decay predicted in [4, Fig. 6.3.2].

As an example of how PPEs might affect product retrieval, Fig. 3 shows an MCI map, calculated using (1). Gower *et al.* [9] already ascertained that a high amount of isolated MCI false alarms were produced in the region affected by the SAA, and they attributed this phenomenon to PPEs. What is shown in Fig. 3 clearly endorses this assertion, as in the uncorrected subscene [Fig. 3(b)], isolated across-track stripes of probably unnatural extremely low/high MCI values are observed (upto 15 mW/nm/sr/m^2 in the worse cases). After the PPE removal scheme, these isolated extreme values tend to be smoothed out, as shown in Fig. 3(c). This same behavior is observed throughout the entire set of selected images from the SAA region.

V. Conclusion

In this letter, a scheme for detection and removal of PPEs from L1B OLCI ocean color images is proposed. It is based on a pixel-by-pixel moving along-track 5×1 kernel and it is applied to all bands. As predicted, it was observed that PPEs affect on average 27.8 times more pixels inside the SAA than in other geographical regions. The absolute errors in TOA radiances induced by PPEs follow a similar pattern to that predicted by D'Amico *et al.* [4], i.e., a shifted exponential decay probability density function, of e-folding of 1 and initial shift of 0.81 mW/nm/sr/m^2 [4]. As an example of how PPEs might induce product retrieval failure, Gower *et al.* [9] alerted for the presence of anomalous isolated MCI alarms, especially in the region the SAA. It is shown how these false isolated alarms will be markedly reduced by applying the PPE-removal scheme over L1B imagery. Despite the fact that PPEs are highly unlikely outside the SAA region, the probability of occurrence are not reduced to zero. Taking this into account and the fact that the geomagnetic field is not stationary, it is recommended to apply the described PPE-removal scheme over all the L1B imagery, and not just over the South Atlantic region. The proposed algorithm can be easily extended to other PPE-sensitive sensors flying on LOEs.

Acknowledgment

The author would like to thank K. G. Ruddick, A. I. Dogliotti, F. M. Grings, J. Nieke, F. D'Amico, and two anonymous reviewers for very helpful comments.

References

[1] G. D. Badhwar, V. V. Kushin, Y. A. Akatov, and V. A. Myltseva, "Effects of trapped proton flux anisotropy on dose rates in low Earth orbit," *Radiat. Meas.*, vol. 30, no. 3, pp. 415–426, Jun. 1999.

[2] Sentinels. *Copernicus*. Accessed: Feb. 14, 2018. [Online]. Available: https://sentinels.copernicus.eu

[3] T. E. Cravens, *Physics of Solar System Plasmas*. Cambridge, U.K.: Cambridge Univ. Press, 1997.

[4] F. D'Amico, G. Corsini, M. Diani, and J. Nieke, "Prompt-particle-events in ESA's Envisat/MERIS and Sentinel-3/OLCI data: Observations, analysis and recommendations," M.S. thesis, Dipartimento Ingegneria dell'Informazione, Univ. Pisa, Pisa, Italy, 2015.

[5] *NASA's Earth Observatory*. Accessed: Feb. 22, 2018. [Online]. Available: https://earthobservatory.nasa.gov/IOTD/view.php?id=84266

[6] EUMETSAT Official Website. *Copernicus Online Data Access*. Accessed: Feb. 3, 2018. [Online]. Available: https://eumetsat.int/website/home/Data/DataDelivery/CopernicusOnlineDataAccess/index.html

[7] ESA Official Website. (2014). *European Space Agency*. [Online]. Available: https://esa.int/spaceinimages/Images/2013/09/Cloud_cover_Thales_Alenia_Space

[8] J. F. R. Gower, C. Hu, G. A. Borstad, and S. King, "Ocean color satellites show extensive lines of floating Sargassum in the Gulf of Mexico," *IEEE Trans. Geosci. Remote Sens.*, vol. 44, pp. 3619–3625, 2006.

[9] J. Gower, S. King, and P. Goncalves, "Global monitoring of plankton blooms using MERIS MCI," *Int. J. Remote Sens.*, vol. 29, no. 21, pp. 6209–6216, 2008, doi: 10.1080/01431160802178110.

[10] J. Nieke *et al.*, "Ocean and land colour imager on Sentinel-3," in *Optical Payloads for Space Missions*, S.-E. Qian, Ed. Hoboken, NJ, USA: Wiley, ch. 10, pp. 223–245.

[11] P. A. Sturrock, J. A. Klimchuk, G. Roumeliotis, and S. K. Antiochos, "The asymptotic behavior of force-free magnetic-field configurations," in *Proc. 14th Int. Summer Workshop, Nat. Sol. Observatory*, vol. 68, Sunspot, NM, USA, Aug./Sep. 1993, pp. 219–224.

IEEE Proof